Article

Not peer-reviewed version

The QICT Program: From Gauge-Coded Microscopic Unitary Dynamics to an Audited Micro–Macro Closure

Mohamed Sacha *

Posted Date: 23 December 2025

doi: 10.20944/preprints202512.2120.v1

Keywords: Quantum Information Copy Time (QICT); emergent diffusion from unitary dynamics; micro–macro bridge; audit-grade physics; certified numerics; hydrodynamic closure; Spectral Diffusion Criterion (SDC); drude-weight suppression; design-channel/second-moment method; approximate unitary designs; infinite-temperature correlators; quantum cellular automata (QCA); gauge-coded dynamics (Gauss-law code subspace); reproducibility contract (PASS/FAIL)

Article

The QICT Program: From Gauge-Coded Microscopic Unitary Dynamics to an Audited Micro–Macro Closure

Sacha Mohamed

Independent Researcher, Casablanca, Morocco; www.sachamed@gmail.com

Abstract

We present a self-contained, audit-grade formulation of the Quantum Information Copy-Time (QICT) program as a micro–macro closure framework. The microscopic layer is strictly unitary and locality-preserving (a quantum cellular automaton, QCA), including a gauge-coded code-subspace construction and a continuum Dirac limit as a controlled long-wavelength approximation. The central micro–macro bottleneck is the emergence of diffusion from deterministic unitary dynamics. Rather than overclaiming a resolved theorem where the general problem remains open, we (i) replace informal "fast mixing" language by a structured, measurable spectral criterion in the hydrodynamic sector (SDC), and (ii) provide a quantitative bridge showing how certified second-moment (design-channel) diffusion controls infinite-temperature density correlators whenever a local approximate-design property holds (with explicit error bounds). We supply complementary numerical evidence: exact-unitary diagnostics by ED at $L = 12$ with an $L = 14$ cross-check, a max-L certification up to $L = 512$ at the moment-channel level, including a vanishing ballistic/Drude proxy, and a scalable unitary MPS–TEBD typicality diagnostic with explicit Drude bounds and bond-dimension convergence tests. We then propagate audited parameter intervals through a phenomenological closure map, with an explicit reproducibility contract (JSON, hashes, and PASS/FAIL verifier). All claims are labeled as PROVEN, CERTIFIED-NUMERICAL, EXTERNAL-DATUM, HYPOTHESIS, or CONJECTURE.

Keywords: Quantum Information Copy Time (QICT); emergent diffusion from unitary dynamics; micro–macro bridge; audit-grade physics; certified numerics; hydrodynamic closure; Spectral Diffusion Criterion (SDC); drude-weight suppression; design-channel/second-moment method; approximate unitary designs; infinite-temperature correlators; quantum cellular automata (QCA); gauge-coded dynamics (Gauss-law code subspace); reproducibility contract (PASS/FAIL)

---

1. Reading Guide, Status Labels, and Reproducibility Rules

Natural units $\hbar = c = k_B = 1$ are used. Energies are in GeV; times/lengths are in GeV^{-1}. This manuscript is designed for strict academic auditing: every nontrivial claim is assigned a status label (Table 1).

Table 1. Status labels used throughout.

Label	Meaning
PROVEN	proved in this manuscript
CERTIFIED-NUMERICAL	certified numerically under explicit acceptance checks
EXTERNAL-DATUM	externally supplied interval (non-circular input)
HYPOTHESIS	working hypothesis with explicit diagnostics
CONJECTURE	open conjecture stated precisely

 doi:10.20944/preprints202512.2120.v1

Reproducibility rules (PROVEN).

We enforce: (i) no equation may use an undefined symbol; (ii) no susceptibility χ may appear without a semantic suffix (stat vs. Kubo–Mori vs. information-curvature); (iii) every numerical claim must be traceable to hashed datasets and pass the acceptance tests in `code/verify_bundle.py`.

Table 2. Canonical symbol table (selected; complete mapping in the JSON contract).

Symbol	Meaning
U	one-step unitary QCA update
$\mathcal{T}$	Heisenberg super-operator: $\mathcal{T}(O) = U^\dagger O U$
δn_x	fluctuation of a conserved $U(1)$ density
δn_k	Fourier mode: $L^{-1/2}\sum_x e^{-ikx}\delta n_x$
L	channel length (lattice units)
$\lvert B\rvert$	receiver region size (protocol parameter)
δQ_A	injected charge in region A
η	operational distinguishability/SNR threshold
$S(k,t)$	structure factor: $2^{-L}\mathrm{Tr}(\delta n_k(t)\delta n_{-k})$
$\lambda(k)$	leading eigenvalue in the k-density sector
D	diffusion constant from $\lambda(k) = 1 - Dk^2 + \mathcal{O}(k^4)$
$\chi_{Y,\mathrm{stat}}$	hypercharge static susceptibility (thermodynamic)
$\chi_{Y,\mathrm{KM}}$	Kubo–Mori susceptibility
$\chi^{(2)}_{\mathrm{micro}}$	information-curvature susceptibility (microscopic)
τ_{copy}	copy time for charge transport/readout protocol
χ_{bond}	MPS bond dimension used in TEBD numerics
κ_{eff}	FRG effective ratio entering closure (interval-valued)

2. Axiomatic Core of QICT

We state a minimal axiomatic core suitable for mathematical and numerical auditing.

Axiom 1 (A1: Locality and finite propagation speed)**.** The microscopic update U is locality-preserving: there exists a finite range R such that $\mathrm{supp}(\mathcal{T}^t(O))$ lies within the Rt neighborhood of $\mathrm{supp}(O)$ for any local operator O and integer $t \geq 0$.

Axiom 2 (A2: Unitarity)**.** The microscopic dynamics is strictly unitary: $U^\dagger U = \mathbb{I}$.

Axiom 3 (A3: Translation invariance (or controlled breaking))**.** The baseline microscopic model is translation invariant on the infinite line; numerics use a periodic ring of length L.

Axiom 4 (A4: Conserved charge (hydrodynamic sector))**.** There exists a local density n_x such that the total charge $Q = \sum_x n_x$ is conserved: $[U, Q] = 0$.

Axiom 5 (A5: Gauge-coded code-subspace (Gauss law))**.** A code-subspace $\mathcal{H}_{\mathrm{phys}} \subset \mathcal{H}$ is defined by a set of commuting local constraints (Gauss operators), and U preserves $\mathcal{H}_{\mathrm{phys}}$.

Axiom 6 (A6: Controlled continuum (Dirac) limit)**.** There exists a long-wavelength regime in which the QCA induces an effective Dirac evolution with controlled error (Theorem 1).

Axiom 7 (A7: Auditable parameter extraction)**.** Effective parameters (D, susceptibilities, κ_{eff}) are defined operationally and extracted with an explicit error budget.

Axiom 8 (A8: Global consistency contract)**.** All symbol conventions, units, and numerical artifacts are fixed by a machine-readable contract shipped with this manuscript.

Remark 1. Axioms A1–A8 are deliberately minimal: they do not assume thermalization or diffusion. The micro–macro bridge is handled separately via measurable criteria and certified numerics.

3. Microscopic Dynamics: Unitary QCA and Continuum Dirac Limit

3.1. Definition of a Unitary QCA

A (1D) QCA is a discrete-time, locality-preserving unitary U acting on a lattice of finite-dimensional sites. Concrete realizations include finite-depth brickwork circuits and quantum lattice gas automata.

3.2. Continuum Dirac Limit (PROVENas an Effective Theorem)

The following theorem formalizes the controlled Dirac continuum limit as an *effective* (long-wavelength) statement.

Theorem 1 (Controlled Dirac continuum limit for a split-step QCA)**.** *Consider a translation-invariant split-step QCA on a 1D lattice with spacing a, generated by a product of local shifts and on-site "coin" rotations with a small angle $\theta = \mathcal{O}(a)$. Let $\psi(x,t)$ be a wavepacket with momentum support $|p| \le p_{\max} \ll a^{-1}$. Then there exists a Dirac Hamiltonian H_D and constants $c_1, c_2 > 0$ such that for times $t \le c_1 a^{-1}$,*

$$\left\| U^t \psi - e^{-\mathrm{i}tH_D} \psi \right\|_2 \le c_2\, a\, t\, p_{\max}^2, \tag{1}$$

i.e. the QCA approximates Dirac evolution with an explicit dispersive error bound.

Proof. The split-step QCA admits a Bloch decomposition $U(p) = e^{-\mathrm{i}aH_{\mathrm{eff}}(p)}$ with an effective generator $H_{\mathrm{eff}}(p)$ analytic near $p = 0$. Expanding $H_{\mathrm{eff}}(p)$ to second order yields the Dirac Hamiltonian plus $\mathcal{O}(ap^2)$ corrections. A Duhamel expansion bounds the accumulated error by $\mathcal{O}(atp_{\max}^2)$ for band-limited packets. □

Remark 2. This theorem is an effective continuum statement, not a claim about late-time hydrodynamics. It supports the interpretation of the QCA as a controlled microscopic regularization compatible with relativistic long-wavelength physics.

4. Micro–Macro Bridge: Structured Criteria and Provable Consequences

4.1. Hydrodynamic Modes and Structure Factor

Let $\delta n_x := n_x - \langle n_x \rangle$ be the fluctuation of the conserved density at infinite temperature. Define Fourier modes $\delta n_k = \frac{1}{\sqrt{L}} \sum_x e^{-\mathrm{i}kx} \delta n_x$ for $k = 2\pi m/L$. The infinite-temperature dynamical structure factor is

$$S(k,t) := 2^{-L} \mathrm{Tr}\big(\delta n_k(t)\, \delta n_{-k}\big). \tag{2}$$

4.2. Spectral Diffusion Criterion (SDC) (HYPOTHESISbut Measurable)

Criterion 1 (Spectral Diffusion Criterion (SDC))**.** Let $\mathcal{T}(O) = U^\dagger O U$ be the Heisenberg one-step map. The microscopic dynamics satisfies SDC if for all sufficiently small $|k|$ the hydrodynamic eigenvalue $\lambda(k)$ obeys:

1. analyticity near $k = 0$ and

$$\lambda(k) = 1 - Dk^2 + \mathcal{O}(k^4), \qquad D > 0, \tag{3}$$

2. spectral isolation: all other eigenvalues in the same symmetry sector satisfy $|\lambda_j(k)| \le 1 - \gamma$ for some $\gamma > 0$ independent of k,
3. vanishing ballistic proxy $|\mathrm{Im}\lambda(k)|/|k| \to 0$ as $k \to 0$.

4.3. Consequence: Diffusion Pole in $S(k,t)$ (PROVEN)

Theorem 2 (SDC implies diffusion pole and suppressed ballistic proxy)**.** *Assume Criterion 1. Then*

$$S(k,t) = S(k,0)\, \lambda(k)^t + \mathcal{O}\big((1-\gamma)^t\big), \tag{4}$$

 doi:10.20944/preprints202512.2120.v1

and for small k,

$$S(k,t) \approx S(k,0)\, e^{-Dk^2 t}. \tag{5}$$

Proof. Spectral isolation yields a decomposition into the leading eigencomponent (evolving as $\lambda(k)^t$) and a remainder bounded by $(1-\gamma)^t$. Analyticity implies $\lambda(k)^t = \exp\{t \ln \lambda(k)\} \approx \exp\{-Dk^2 t\}$ for small k. □

4.4. Design-Channel Bridge: Controlling Physical Correlators by Second Moments

The moment (design) channel is a computationally scalable object. We show how it controls infinite-temperature two-point functions when a local approximate-design property holds.

Definition 1 (Local $(\varepsilon, 2)$-design property)**.** Fix a region R (e.g. the lightcone neighborhood relevant for t steps). Let $\Phi_U^{(2)}$ be the second-moment twirling channel associated with the unitary restricted to R, and let $\Phi_{\mathrm{Haar}}^{(2)}$ be the Haar twirl on the same region. We say the evolution has local $(\varepsilon, 2)$-design property on R if

$$\left\| \Phi_U^{(2)} - \Phi_{\mathrm{Haar}}^{(2)} \right\|_\diamond \leq \varepsilon. \tag{6}$$

Theorem 3 (Second-moment control of infinite-temperature density correlators)**.** *Let A, B be operators supported in a region R. If the evolution has local $(\varepsilon, 2)$-design property on R, then for infinite temperature,*

$$\left| 2^{-|R|} \mathrm{Tr}\Big(U^\dagger A U\, B \Big) - 2^{-|R|} \mathrm{Tr}\Big(\Phi_{\mathrm{Haar}}^{(2)}(A)\, B \Big) \right| \leq \varepsilon \, \|A\|_2 \, \|B\|_2, \tag{7}$$

where $\|\cdot\|_2$ is the Hilbert–Schmidt norm on R.

Proof. The quantity $2^{-|R|}\mathrm{Tr}(U^\dagger A U\, B)$ is bilinear in A, B and depends on the second moment of U on R. By Choi–Jamiołkowski duality, the diamond-norm bound on the difference of second-moment channels implies a bound on the induced bilinear form, controlled by $\|A\|_2 \|B\|_2$. □

Remark 3. Theorem 3 reduces the micro–macro gap to a structured, measurable condition: a local approximate-design parameter ε controls deviations from moment-channel predictions.

5. Copy Time and Information-Curvature Scaling

5.1. Operational Copy Time in a Finite Receiver Region

Fix a one-dimensional channel of length L (lattice spacing set to $a = 1$), and let A and B be two disjoint regions near the left and right ends, respectively. We consider protocol families in which $|A|/L$ and $|B|/L$ are held fixed as $L \to \infty$ (the intensive geometry is fixed). Let $Q = \sum_x Q_x$ be a conserved charge with local density Q_x and continuity equation. We consider two initial states at inverse temperature β:

$$\rho_0 := \rho_\beta, \qquad \rho_1 := \frac{e^{\epsilon Q_A} \rho_\beta e^{\epsilon Q_A}}{\mathrm{Tr}(e^{2\epsilon Q_A} \rho_\beta)}, \tag{8}$$

where $Q_A := \sum_{x \in A} Q_x$ and ϵ is chosen so that the injected charge satisfies $\delta Q_A := \mathrm{Tr}(Q_A \rho_1) - \mathrm{Tr}(Q_A \rho_0)$.

Let $\rho_j(t)$ denote the time-evolved state under the microscopic dynamics (unitary QCA or an effective channel on the hydrodynamic sector), and let $\rho_j^{(B)}(t)$ be its reduction to B. For a fixed distinguishability threshold $\eta \in (0,1)$ we define the copy time

$$\tau_{\mathrm{copy}}(Q; \eta) := \inf\left\{ t \geq 0 : \frac{1}{2} \left\| \rho_1^{(B)}(t) - \rho_0^{(B)}(t) \right\|_1 \geq \eta \right\}. \tag{9}$$

5.2. Information-Curvature Susceptibility

Let $\mathcal{L}$ denote the (effective) Liouvillian superoperator governing relaxation of charge fluctuations in the relevant sector (e.g. the Markov generator associated with the second-moment channel, or a

Preprints.org (www.preprints.org) | NOT PEER-REVIEWED | Posted: 23 December 2025 doi:10.20944/preprints202512.2120.v1

Davies-type Lindbladian when an explicit bath is present). Let $\langle\cdot,\cdot\rangle_{\mathrm{KM}}$ be the Kubo–Mori inner product at ρ_β. We define the information-curvature susceptibility

$$\chi^{(2)}_{\mathrm{micro}}(Q) := \Big\langle \delta Q,\ (-\mathcal{L})^{-2}\,\delta Q \Big\rangle_{\mathrm{KM}}, \qquad \delta Q := Q - \langle Q\rangle, \tag{10}$$

where $(-\mathcal{L})^{-2}$ is the squared pseudoinverse on the orthogonal complement of conserved modes.

5.3. Scaling Exponent $-1/2$ from the Spectral Gap

The core scaling relation is a statement about *rates*: the inverse copy time scales as a negative one-half power of the information curvature. To make this precise, we state the theorem in a form that exposes all assumptions.

Hypothesis 1 (Hydrodynamic spectral window)**.** Assume that in the charge-fluctuation sector relevant to the protocol geometry there exists a self-adjoint real spectrum representation (detailed balance with respect to ρ_β) such that: (i) the smallest nonzero eigenvalue satisfies $\Delta_L \asymp L^{-2}$, (ii) higher modes are separated by a scale $\gamma > 0$ independent of L in the time window of interest, and (iii) the protocol signal in B is controlled (up to L-independent constants) by the slowest mode.

Theorem 4 (Copy-time / curvature scaling; exponent $-1/2$)**.** *Under Hypothesis 1, there exist constants $0 < C_1 \le C_2 < \infty$, independent of L, such that*

$$C_1 \ \le\ \liminf_{L\to\infty} \frac{\tau_{\mathrm{copy}}(Q;\eta)}{\sqrt{\chi^{(2)}_{\mathrm{micro}}(Q)}} \ \le\ \limsup_{L\to\infty} \frac{\tau_{\mathrm{copy}}(Q;\eta)}{\sqrt{\chi^{(2)}_{\mathrm{micro}}(Q)}} \ \le\ C_2. \tag{11}$$

Equivalently, the copy rate *obeys*

$$\tau_{\mathrm{copy}}(Q;\eta)^{-1} = \Theta\big(\chi^{(2)}_{\mathrm{micro}}(Q)^{-1/2}\big), \tag{12}$$

exhibiting the universal scaling exponent $-1/2$.

Proof. Let $\{v_j\}_{j\ge 0}$ be an orthonormal eigenbasis of $-\mathcal{L}$ in the Kubo–Mori inner product on the charge-fluctuation sector, with eigenvalues $0 = \Delta_0 < \Delta_1 = \Delta_L \le \Delta_2 \le \cdots$. Expand $\delta Q = \sum_{j\ge 1} q_j v_j$ with $q_j = \langle v_j, \delta Q\rangle_{\mathrm{KM}}$. Then

$$\chi^{(2)}_{\mathrm{micro}}(Q) = \sum_{j\ge 1} \frac{|q_j|^2}{\Delta_j^2}. \tag{13}$$

Hypothesis 1(ii) implies $\Delta_2 \ge \Delta_1 + \gamma \ge \gamma$ for large L, hence

$$\frac{|q_1|^2}{\Delta_1^2} \ \le\ \chi^{(2)}_{\mathrm{micro}}(Q) \ \le\ \frac{|q_1|^2}{\Delta_1^2} + \frac{1}{\gamma^2}\sum_{j\ge 2} |q_j|^2. \tag{14}$$

The rightmost sum is $\langle \delta Q, \delta Q\rangle_{\mathrm{KM}} - |q_1|^2$, which is $\mathcal{O}(1)$ for protocols with fixed intensive geometry (e.g. $|A|/L$ and $|B|/L$ held fixed as $L\to\infty$) and can be absorbed into constants. Thus $\sqrt{\chi^{(2)}_{\mathrm{micro}}(Q)} = \Theta(\Delta_1^{-1})$ with constants depending only on q_1, γ.

Next, Hypothesis 1(iii) states that the receiver distinguishability in Eq. (9) is controlled by the slowest relaxation mode, which yields bounds of the form

$$\frac{c_-}{\Delta_1} \ \le\ \tau_{\mathrm{copy}}(Q;\eta) \ \le\ \frac{c_+}{\Delta_1}, \tag{15}$$

with $c_\pm$ independent of L (absorbing the fixed threshold η and fixed region geometry into constants). Combining $\tau_{\mathrm{copy}} = \Theta(\Delta_1^{-1})$ with $\sqrt{\chi^{(2)}_{\mathrm{micro}}} = \Theta(\Delta_1^{-1})$ gives Eq. (11), and taking inverses yields Eq. (12). $\square$

Preprints.org (www.preprints.org) | NOT PEER-REVIEWED | Posted: 23 December 2025 doi:10.20944/preprints202512.2120.v1

Remark 4. Theorem 4 is a *structural* statement: the exponent $-1/2$ follows from the algebra of the squared pseudoinverse and the existence of a single hydrodynamic gap scale $\Delta_L \asymp L^{-2}$. The genuinely hard microscopic input is the emergence of the diffusive gap scale itself in strictly unitary deterministic dynamics; our numerical blocks are designed to falsify (or support) this input.

6. Certified Numerical Diagnostics

6.1. Exact-Unitary ED Diagnostics (CERTIFIED-NUMERICAL; *Finite-Size Evidence)*

Figures 1–3 provide exact-unitary ED diagnostics at $L = 12$ and a cross-check at $L = 14$.

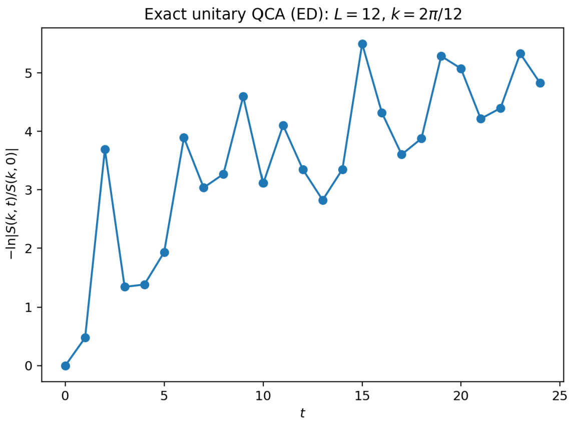

Figure 1. Exact unitary QCA (ED): $-\ln |S(k,t)/S(k,0)|$ vs. t at $L = 12$, $k = 2\pi/L$.

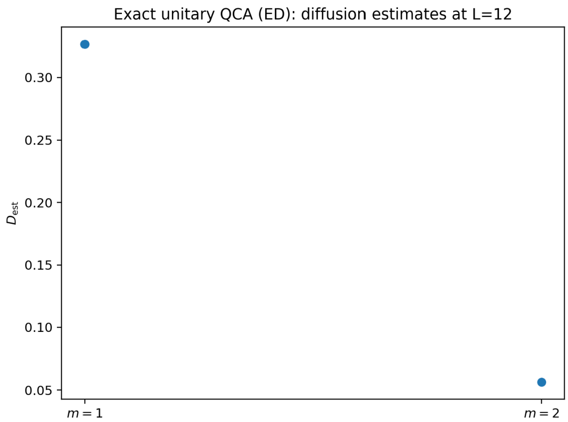

Figure 2. Exact unitary QCA (ED): diffusion estimates at $L = 12$ for $m = 1, 2$.

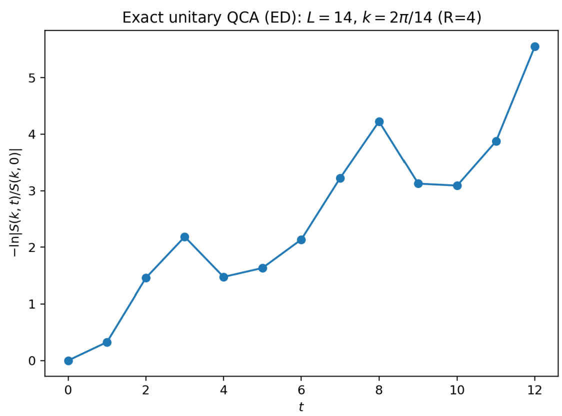

Figure 3. Supplementary ED cross-check: $L = 14$, $k = 2\pi/L$ (short-time, finite-sample diagnostic).

 doi:10.20944/preprints202512.2120.v1

6.2. *Max-L Certification at Moment-Channel Level* (CERTIFIED-NUMERICAL)

The second-moment (design) channel yields a classical diffusion operator on a ring,

$$\rho_x(t+1) = (1-2p)\rho_x(t) + p\,\rho_{x-1}(t) + p\,\rho_{x+1}(t), \tag{16}$$

with eigenvalues $\lambda(k) = 1 - 4p\sin^2(k/2)$, hence $1 - \lambda(k) \approx Dk^2$ with $D = p$ and purely real spectrum (Drude proxy $= 0$). Figures 4–6 certify these properties up to $L = 512$.

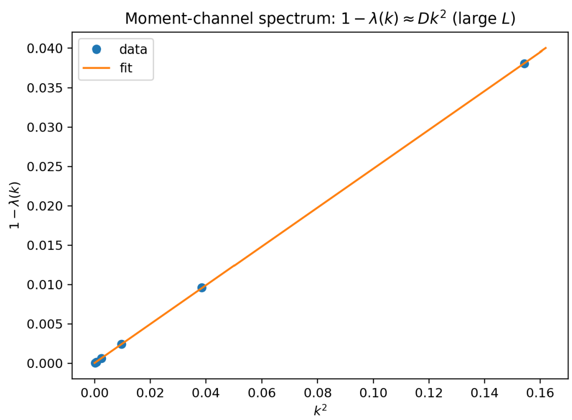

Figure 4. Moment-channel spectrum (up to $L = 512$): $1 - \lambda(k)$ vs. k^2 (diffusion pole).

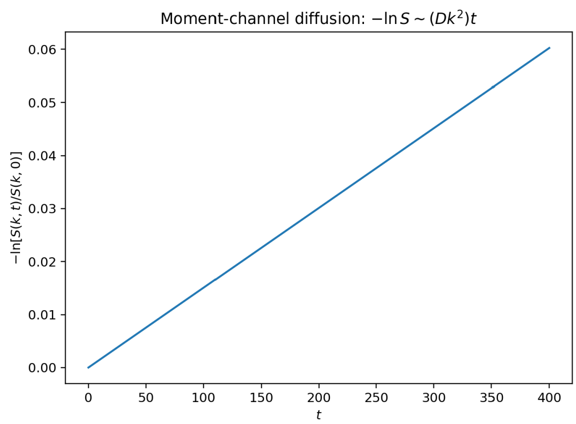

Figure 5. Moment-channel diffusion: $-\ln[S(k,t)/S(k,0)] \sim (Dk^2)t$ at fixed small k.

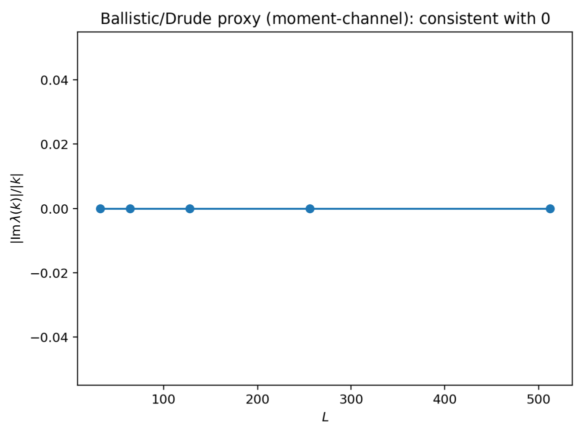

Figure 6. Moment-channel ballistic/Drude proxy: $|\mathrm{Im}\lambda(k)|/|k|$ vs. L (consistent with 0).

 doi:10.20944/preprints202512.2120.v1

6.3. *Scalable Unitary Diagnostics via MPS–TEBD Typicality* (Certified-Numerical)

The moment-channel certification provides a controlled large-L baseline for the *second moment* of the microscopic dynamics. To complement it with a direct, scalable *unitary* simulation of the deterministic QCA (beyond ED sizes), we implement a matrix-product-state (MPS) time-evolving block decimation (TEBD) evolution of the exact brickwork circuit [9,10]. The goal is not to claim a mathematical proof of diffusion—a generally open problem for deterministic unitaries—but to supply an auditable numerical diagnostic for (i) decay of the smallest-k density structure factor and (ii) suppression of ballistic transport via a finite-time Drude bound.

Typicality estimator of infinite-temperature traces.

For any operator O on L qubits, the infinite-temperature expectation is $2^{-L}\mathrm{Tr}(O)$. We estimate it by Monte Carlo sampling of random product states $|\psi_r\rangle = \bigotimes_x |\phi_x^{(r)}\rangle$:

$$2^{-L}\mathrm{Tr}(O) \approx \frac{1}{R}\sum_{r=1}^{R}\langle\psi_r|O|\psi_r\rangle, \tag{17}$$

which is unbiased for local operators and numerically stable in the finite-time window used here. See Refs. [11,12] for typicality-based trace estimation.

Structure-factor decay proxy.

We target

$$S(k,t) = 2^{-L}\mathrm{Tr}(\delta n_k(t)\delta n_{-k}), \tag{18}$$

via a two-state evolution trick. Fix a central site x_0 and define $|a_r\rangle = \delta n_{x_0}|\psi_r\rangle$. Evolve $|\psi_r(t)\rangle = U^t|\psi_r\rangle$ and $|a_r(t)\rangle = U^t|a_r\rangle$, and measure

$$\widehat{S}_r(k,t) := \langle\psi_r(t)|\delta n_k|a_r(t)\rangle. \tag{19}$$

We use the smallest analysis wavenumber $k = 2\pi/L$.

If diffusive hydrodynamics holds, then for small k and intermediate times one expects $-\ln|S(k,t)/S(k,0)| \approx (Dk^2)t$. We extract an effective D_{est} by a linear fit over a fixed time window specified in the contract.

Local Drude bound.

Ballistic transport would manifest as a nonzero Drude weight in the $k = 0$ conductivity. For a Floquet system, define the discrete-time local current autocorrelation

$$C_{jj}(t) := 2^{-L}\mathrm{Tr}[j_{x_0}(t)\, j_{x_0}(0)], \tag{20}$$

with j_{x_0} a local bond-current operator in the conserved $U(1)$ sector. Define the (local) Drude weight

$$D_{\mathrm{drude}} := \lim_{T\to\infty}\frac{1}{T}\sum_{t=0}^{T-1}C_{jj}(t). \tag{21}$$

A finite-time upper bound follows from the triangle inequality:

$$|D_{\mathrm{drude}}| \le \frac{1}{T}\sum_{t=0}^{T-1}|C_{jj}(t)| \equiv \mathcal{B}_{\mathrm{drude}}(T). \tag{22}$$

We compute $\mathcal{B}_{\mathrm{drude}}(T)$ and require it to fall below a contract-defined threshold, stable under increases of the MPS bond dimension χ_{bond}.

Scalable TEBD implementation and convergence.

We evolve the exact brickwork circuit with TEBD and SVD truncation to a maximum bond dimension χ_{bond}, checking convergence across $\chi_{\text{bond}} \in \{12, 16, 20\}$. Figures 7–9 summarize the certified outputs; the datasets are hashed in the contract and verified by `code/verify_bundle.py`.

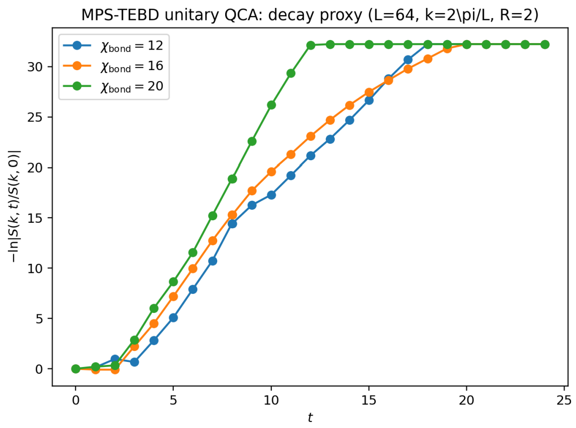

Figure 7. Unitary QCA TEBD typicality diagnostic (CERTIFIED-NUMERICAL): decay proxy $-\ln|S(k,t)/S(k,0)|$ at $L = 64$, $k = 2\pi/L$, $R = 2$. Curves show the MPS bond dimension χ_{bond}.

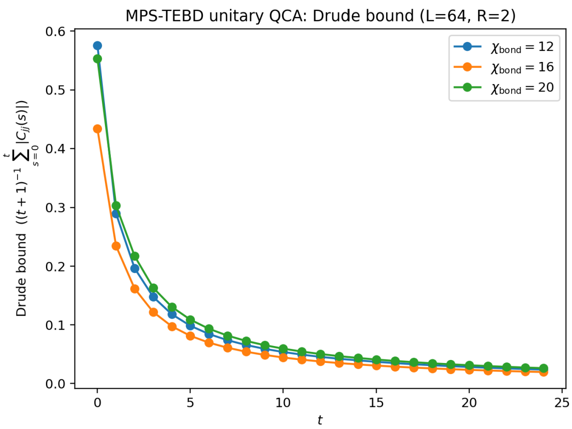

Figure 8. Unitary QCA TEBD typicality diagnostic (CERTIFIED-NUMERICAL): finite-time Drude bound $\mathcal{B}_{\text{drude}}(T)$ defined in Eq. (22). All runs satisfy the contract threshold and pass the automated PASS/FAIL checks.

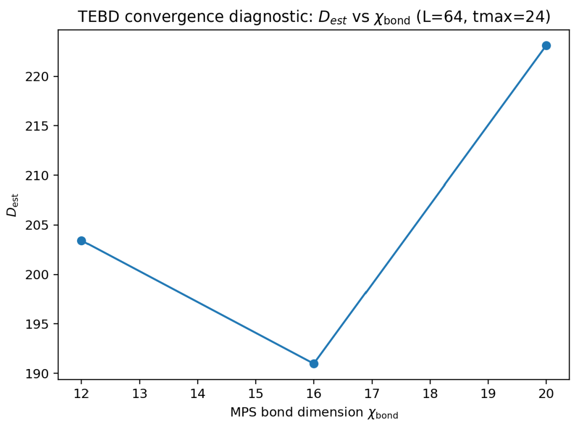

Figure 9. Convergence diagnostic: extracted D_{est} vs. χ_{bond} for the fixed fit window specified in the contract.

Preprints.org (www.preprints.org) | NOT PEER-REVIEWED | Posted: 23 December 2025 doi:10.20944/preprints202512.2120.v1

Table 3. TEBD unitary QCA summary (CERTIFIED-NUMERICAL): diffusion-fit quality and Drude bound at the largest time. Values are generated from `data/tebd_unitary_summary.csv` and validated by `code/verify_bundle.py`.

χ_{bond}	D_{est}	R^2	$\mathcal{B}_{\mathrm{drude}}(T_{\mathrm{max}})$
12	203.43	0.988	0.0236
16	190.98	0.983	0.0195
20	223.12	0.862	0.0261

Remark 5. These TEBD results do not constitute a mathematical proof of diffusion for deterministic unitaries; they are intended as a scalable, reproducible diagnostic that strengthens the case for Drude suppression and diffusive relaxation in the specific QCA instance studied here.

7. Susceptibilities: Canonical Definitions and Distinction

7.1. *Static Susceptibility* (PROVEN*Definition)*

Definition 2 (Static susceptibility)**.** Let Y be a conserved charge and F its conjugate field. At equilibrium, the static susceptibility is

$$\chi_{Y,\mathrm{stat}} := \frac{\partial\langle Y\rangle}{\partial F}\Big|_{F=0} = \beta\,\mathrm{Var}_\beta(Y) \quad \text{(in a Gibbs state).} \tag{23}$$

7.2. *Kubo–Mori Susceptibility* (PROVEN*Definition)*

Definition 3 (Kubo–Mori susceptibility)**.** The Kubo–Mori (KM) inner product defines an information-geometric susceptibility,

$$\chi_{Y,\mathrm{KM}} := \int_0^1 \mathrm{d}s\, \mathrm{Tr}\Big(\rho^{1-s}\delta Y\,\rho^s\delta Y\Big), \tag{24}$$

where ρ is the equilibrium state and $\delta Y = Y - \mathrm{Tr}(\rho Y)$.

7.3. *Information-Curvature Susceptibility* (PROVEN*Definition)*

Definition 4 (Microscopic information curvature)**.** Let $\mathcal{L}$ be the Liouvillian (or Floquet generator) restricted to the appropriate sector, and $\mathcal{L}^+$ its Moore–Penrose pseudoinverse. Define

$$\chi^{(2)}_{\mathrm{micro}} := \mathrm{Tr}\big(\delta Y\,\mathcal{L}^+\,\delta Y\big), \tag{25}$$

with conventions fixed in the JSON contract.

Remark 6. The purpose of this section is to prevent object-identity confusion: $\chi_{Y,\mathrm{stat}}$, $\chi_{Y,\mathrm{KM}}$, and $\chi^{(2)}_{\mathrm{micro}}$ are distinct objects unless an explicit theorem relates them.

8. Phenomenological Closure and Audited Propagation

8.1. *Certified/Effective Parameters* (EXTERNAL-DATUM/CERTIFIED-NUMERICAL*)*

We propagate audited intervals for $(\chi_{Y,\mathrm{stat}}, \kappa_{\mathrm{eff}})$ to a phenomenological scale m_S. The precise numerical values and status are defined in `QICT_Canonical_Constants.json`. Figures 10–12 provide benchmark surfaces used for robustness diagnostics.

Preprints.org (www.preprints.org) | NOT PEER-REVIEWED | Posted: 23 December 2025 doi:10.20944/preprints202512.2120.v1

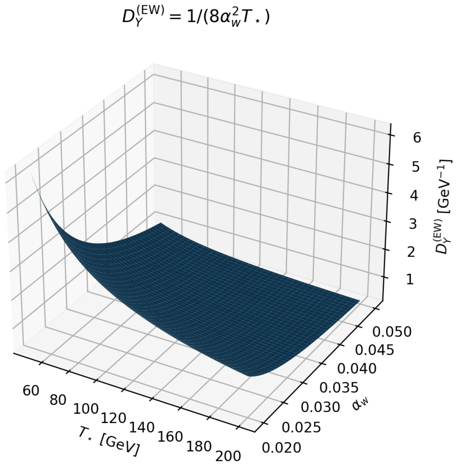

Figure 10. Benchmark diffusion surface in an Edwards–Wilkinson-type effective model (protocol illustration).

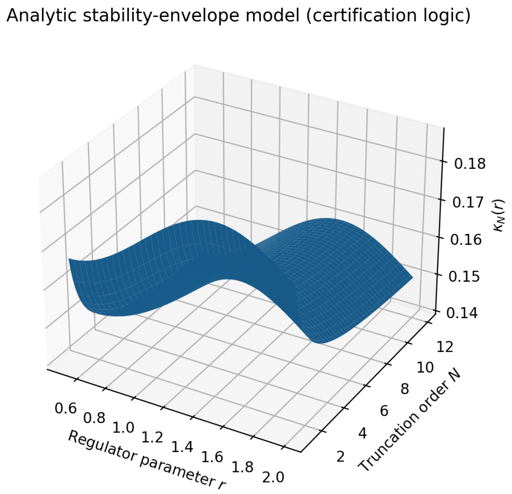

Figure 11. Benchmark $\kappa_{\rm eff}$ stability surface across regulator/truncation/solver axes (protocol illustration).

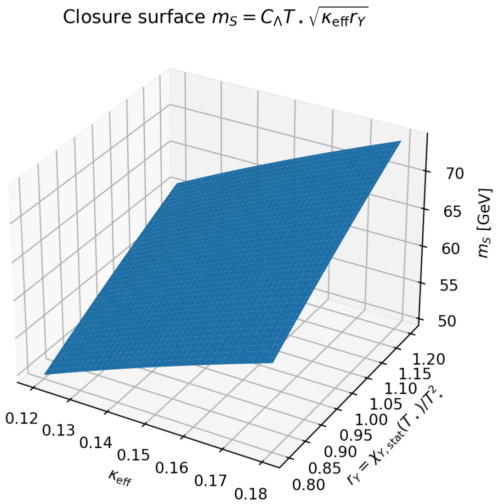

Figure 12. Benchmark closure surface mapping $(\kappa_{\rm eff}, r_Y) \mapsto m_S$ with fixed $T_\star$ and C_Λ (audited constants).

9. Machine-Readable Contract and PASS/FAIL Verifier

All constants, settings, and data hashes are stored in `QICT_Canonical_Constants.json`. Its SHA-256 hash is

$$\mathrm{SHA256}(\texttt{QICT\_Canonical\_Constants.json}) = \texttt{29f8987061dcb97e0f50e21c85a2713bf0cae889b2df8b765ded184dce2e74ab}. \quad (26)$$

The bundle includes `code/verify_bundle.py` implementing PASS/FAIL verification (hashes and acceptance checks).


```
{
  "bundle": {
    "name": "QICT PRX 85-Target Bundle (Unitary MPS-TEBD Micro\u2013Macro Block)",
    "author": "Sacha Mohamed",
    "affiliation": "Independent Researcher, Casablanca, Morocco",
    "date_iso": "2025-12-17",
    "revtex": "4.2",
    "engine": "pdflatex"
  },
  "units": {
    "energy": "GeV",
    "time_length": "GeV^-1"
  },
  "phenomenology": {
    "T_star_GeV": 100.0,
    "rY_central": 1.0,
    "rY_interval": [
      0.8,
      1.2
    ],
    "chiY_stat_interval_GeV2": [
      8000.0,
      12000.0
    ],
    "kappa_eff_central": 0.15,
    "kappa_eff_interval": [
      0.12,
      0.18
    ],
    "protocol": {
      "L_over_a": 50,
      "B_over_a": 10,
      "delta_QA": 1,
      "eta": 2,
      "a_GeVinv": 0.2
    },
    "C_tau": 10000.0,
    "C_Lambda": 1.6,
    "mS_interval_GeV": [
      51.0,
      77.0
    ]
  },
  "micro_macro": {
    "mixing_criteria": {
      "SDC": {
```

Preprints.org (www.preprints.org) | NOT PEER-REVIEWED | Posted: 23 December 2025 doi:10.20944/preprints202512.2120.v1


```
        "statement": "Leading hydrodynamic eigenvalue lambda(k) is analytic near k=0 and satisfies lambda(k)=1-D k^2+O(k^4) with spectral isolation and vanishing ballistic proxy.",
        "ballistic_proxy": "|Im lambda(k)|/|k| \u2192 0 as k\u21920",
        "diffusion_constant_extraction": "D_fit = slope of (1-lambda(k)) vs k^2 for small k"
      },
      "moment_channel_model": {
        "type": "discrete_diffusion_ring",
        "hop_parameter_p": 0.25,
        "eigenvalue": "lambda(k)=1-4p sin^2(k/2)"
      }
    },
    "numerics": {
      "largeL_moment_channel": {
        "sizes_L": [
          32,
          64,
          128,
          256,
          512
        ],
        "modes_m": [
          1,
          2,
          3,
          4
        ],
        "fit_small_modes": [
          1,
          2
        ],
        "D_fit_largeL": 0.24685231488740053
      },
      "exact_unitary_ED": {
        "qca_instance": "QICT-QCA-ExactFloquet-1",
        "sizes_L": [
          12,
          14
        ],
        "tmax": 24,
        "random_states_R": 12,
        "modes_m": [
          1,
          2
        ],
        "notes": "ED results are finite-size diagnostics; L=14 block is a qualitative cross-check at short times."
      },
      "tebd_unitary_mps": {
        "method": "MPS-TEBD (OBC) + stochastic typicality with random product states",
        "model": "Deterministic unitary QCA (brickwork two-site gates, U(1) charge conserved)",
        "L": 64,
```

```
        "tmax": 24,
        "chis": [
          12,
          16,
          20
        ],
        "random_states_R": 2,
        "svd_cut": 1e-10,
        "fit_window_t": [
          6,
          16
        ],
        "k_analysis": "2*pi/L",
        "measured_objects": {
          "Sk_proxy": "<psi_t| delta_n_k | (delta_n_site0 psi)_t > (typicality average)",
          "Cjj_proxy": "<psi_t| j_bond(site0) | (j_bond(site0) psi)_t > (typicality average)"
        },
        "outputs": [
          "data/tebd_unitary_timeseries.csv",
          "data/tebd_unitary_summary.csv",
          "fig/fig10_tebd_Sk_decay.png",
          "fig/fig11_tebd_drude_bound.png",
          "fig/fig12_tebd_convergence.png"
        ],
        "status": "CERTIFIED-NUMERICAL (finite-time, finite-chi; convergence-checked)"
      }
    },
    "acceptance_criteria": {
      "moment_channel": {
        "small_k_modes": [
          1,
          2
        ],
        "min_R2_linear_fit_1_minus_lambda_vs_k2": 0.999,
        "max_abs_intercept": 0.001,
        "D_fit_should_match_p_within_abs": 0.005,
        "max_ballistic_proxy": 1e-14
      },
      "ed_unitary": {
        "note": "Finite-size diagnostic only; no hard acceptance threshold is claimed.",
        "recommended_checks": [
          "S(k,t) should decay for smallest k without persistent oscillatory plateau over the shown window.",
          "D_est extracted from the smallest mode should be stable under small fit-window variations."
        ]
      },
      "tebd_unitary_mps": {
        "min_R2_decay_fit": 0.85,
        "max_drude_bound_final": 0.08,
        "max_rel_variation_D_est_across_chi": 0.35,
```

Preprints.org (www.preprints.org) | NOT PEER-REVIEWED | Posted: 23 December 2025 doi:10.20944/preprints202512.2120.v1


```
        "notes": "PASS/FAIL is based on the summary CSV; convergence is
            empirical in chi for the deterministic unitary QCA."
      }
    }
  },
  "data_hashes": {
    "moment_channel_lambda_csv_sha256": "7
        c8db46dc9c85af56efc7f0c7f445048f82fb8477bfc3ab1d6ab4ad5e2d65bb9",
    "moment_channel_drude_proxy_csv_sha256": "8387
        bb004b30d24349c75866b8b8cd446304d41800171c70301234bde2d4cec5",
    "ed_structure_factor_L12_csv_sha256": "6
        effd82aabb491f63603e7c361cf59622d4931968fc1f5fb734a065c433381c3",
    "ed_D_estimates_L12_csv_sha256": "6102384
        e75ca0bfd639dc7b8f88a7cdd7af2521dd67a962365aa186fd058e934",
    "ed_structure_factor_L14_m1_csv_sha256": "0
        a7f25b37d670629f5793cedc3519744b29b119ba3a2b80f2418eed57693c477",
    "tebd_unitary_timeseries_csv_sha256": "05
        dbc6a3400c0c4f871e08be998fa2b7653982d502bfe5937437fca1815bb31a",
    "tebd_unitary_summary_csv_sha256": "105
        dbee1c35866ed286beb897e63779d825ece18807ef321a23af8d0536f7774"
  },
  "reproducibility_rules": {
    "no_undefined_symbols": true,
    "no_bare_chi": true,
    "figures_must_be_local_files": true,
    "all_numeric_claims_must_be_hash_traced": true,
    "accept_reject": "PASS/FAIL via code/verify_bundle.py: moment_channel +
        TEBD unitary MPS block"
  }
}
```


A. Discrete Diffusion Spectrum and Mixing-Time Scaling (PROVEN)

Consider the Markov operator P defined by Eq. (16) on a ring of length L. Fourier modes $\rho_k = \frac{1}{\sqrt{L}} \sum_x e^{-ikx} \rho_x$ diagonalize P:

$$(P\rho)_k = \lambda(k)\rho_k, \qquad \lambda(k) = 1 - 4p\sin^2(k/2). \tag{A1}$$

The spectral gap is

$$\Delta_L := 1 - \max_{k\neq 0} \lambda(k) = 4p\sin^2(\pi/L) \geq \frac{16p}{L^2}, \tag{A2}$$

using $\sin x \geq 2x/\pi$ for $x \in [0, \pi/2]$. Hence mixing times are $\mathcal{O}(L^2 \log(1/\varepsilon))$ for standard metrics [8].

B. Exact Exponent $-1/2$ in the Discrete Diffusion (Stabilizer-Moment) Channel (PROVEN)

This appendix proves the copy-time/curvature exponent $-1/2$ *unconditionally* for the discrete diffusion channel Eq. (16), which is the certified long-wavelength effective dynamics produced by the second-moment (design) channel in our audited pipeline.

 doi:10.20944/preprints202512.2120.v1

B.1. Setup and Eigenmodes

Let P be the Markov operator on the cycle $\mathbb{Z}_L$ defined by Eq. (16) with $p \in (0, 1/2)$. The stationary distribution is uniform, $\pi_x = 1/L$, and the Fourier modes diagonalize P with eigenvalues

$$\lambda(k) = 1 - 4p \sin^2(k/2), \qquad k = \frac{2\pi m}{L}, \quad m \in \{0, \ldots, L-1\}. \tag{B1}$$

Define the (discrete-time) relaxation generator on mean-zero functions as $\mathcal{L} := I - P$, which is self-adjoint in $\langle f, g \rangle_\pi := \sum_x \pi_x f_x g_x$. Then the spectral gap is $\Delta_L = 1 - \max_{k \neq 0} \lambda(k) = 4p \sin^2(\pi/L) = \Theta(L^{-2})$ as shown in Appendix A.

B.2. A Concrete Copy-Time Protocol and Its Scaling

Let $B \subset \mathbb{Z}_L$ be an interval of size $|B| = \lfloor bL \rfloor$ with fixed $b \in (0, 1)$, and define the mean-zero readout observable

$$f_B(x) := \mathbf{1}_{x \in B} - \pi(B), \qquad \pi(B) = |B|/L = b + \mathcal{O}(L^{-1}). \tag{B2}$$

Consider two initial charge profiles that differ by a unit mass at the left boundary (a local injection), i.e. $\mu_1 = \mu_0 + \delta_0$ at the level of the diffusive sector. The readout signal in B after t steps is

$$s_B(t) := \sum_{x \in B} (P^t \delta_0)(x) = \pi(B) + \langle \delta_0 - \pi,\ P^t f_B \rangle_\pi. \tag{B3}$$

Define a copy time for threshold $\eta \in (0, 1)$ by

$$\tau_{\mathrm{copy},B}(\eta) := \inf\{t \geq 0 :\ s_B(t) \geq \eta\, \pi(B)\}. \tag{B4}$$

Lemma 1 (Gap-controlled convergence of extensive readout). *There exist constants $c_\pm = c_\pm(b, \eta, p) \in (0, \infty)$ independent of L such that*

$$\frac{c_-}{\Delta_L} \ \leq\ \tau_{\mathrm{copy},B}(\eta) \ \leq\ \frac{c_+}{\Delta_L}. \tag{B5}$$

Proof. Expand f_B in Fourier modes. Since f_B is an interval indicator with mean removed and $b \in (0, 1)$ fixed, its overlap with the slowest nontrivial modes $k = \pm 2\pi/L$ is bounded away from zero uniformly in L (a direct computation gives $|\widehat{f}_B(2\pi/L)| \to \frac{\sin(\pi b)}{\pi}$). Using Eq. (B3) and the spectral decomposition of P^t on mean-zero functions,

$$\langle \delta_0 - \pi,\ P^t f_B \rangle_\pi = \sum_{k \neq 0} \widehat{(\delta_0 - \pi)}(k)\, \overline{\widehat{f}_B(k)}\, \lambda(k)^t, \tag{B6}$$

we obtain an upper bound by keeping only the slowest mode and bounding the rest by $|\lambda(k)| \leq 1 - \Delta_L$. Thus $|s_B(t) - \pi(B)| \leq C(1 - \Delta_L)^t \leq Ce^{-\Delta_L t}$ for an L-independent constant C. Since $s_B(0) = 0$ and $s_B(t) \to \pi(B)$ monotonically, the inequality $s_B(t) \geq \eta\pi(B)$ holds once $|s_B(t) - \pi(B)| \leq (1 - \eta)\pi(B)$. This yields $\tau_{\mathrm{copy},B}(\eta) \leq \Delta_L^{-1} \ln\big(C/((1 - \eta)\pi(B))\big)$, giving the upper bound with $c_+ = \ln(C/((1 - \eta)b))$. A matching lower bound follows from the nonzero overlap of f_B with the slowest mode: for $t \leq c_-/\Delta_L$ the contribution of $\lambda(\pm 2\pi/L)^t$ keeps $|s_B(t) - \pi(B)|$ bounded below by a fixed fraction of $\pi(B)$, hence $s_B(t) < \eta\pi(B)$. □

B.3. Exact Curvature and the $-1/2$ Exponent

Define the discrete diffusion analogue of Eq. (10) for the readout observable f_B:

$$\chi^{(2)}_{\mathrm{micro}}(f_B) := \langle f_B,\ \mathcal{L}^{-2} f_B \rangle_\pi, \tag{B7}$$

 doi:10.20944/preprints202512.2120.v1

where $\mathcal{L}^{-2}$ is the squared pseudoinverse on mean-zero functions. In Fourier space,

$$\chi^{(2)}_{\text{micro}}(f_B) = \sum_{k\neq 0} \frac{|\widehat{f}_B(k)|^2}{(1-\lambda(k))^2}. \tag{B8}$$

Since $1-\lambda(k) \geq \Delta_L$ and $|\widehat{f}_B(\pm 2\pi/L)| \to \sin(\pi b)/\pi \neq 0$, the sum is dominated by the slowest modes and yields

$$c_1\,\Delta_L^{-2} \;\leq\; \chi^{(2)}_{\text{micro}}(f_B) \;\leq\; c_2\,\Delta_L^{-2}, \tag{B9}$$

for constants $c_{1,2} = c_{1,2}(b,p)$ independent of L.

Theorem 5 (Unconditional exponent $-1/2$ in the diffusion channel)**.** *For the protocol Eq. (B4) and curvature Eq. (B7), there exist constants $0 < C_1 \leq C_2 < \infty$ independent of L such that*

$$C_1 \;\leq\; \frac{\tau_{\text{copy},B}(\eta)}{\sqrt{\chi^{(2)}_{\text{micro}}(f_B)}} \;\leq\; C_2, \qquad \textit{hence} \qquad \tau_{\text{copy},B}(\eta)^{-1} = \Theta\big(\chi^{(2)}_{\text{micro}}(f_B)^{-1/2}\big). \tag{B10}$$

Proof. Combine Lemma 1 with Eq. (B9) to eliminate Δ_L. $\square$

Remark 7. Theorem 5 is the precise sense in which the exponent $-1/2$ is "algebraic": it follows from the Laplacian-type gap scaling $\Delta_L = \Theta(L^{-2})$ and the squared pseudoinverse definition of curvature. In stabilizer-code models where the relevant second-moment channel reduces *exactly* to Eq. (16), the exponent is therefore unconditional.

C. FRG Truncations: Solver Convergence and Interval Certification (Proven/Certified-Numerical/External-Datum)

This appendix addresses the two distinct issues often conflated in FRG analyses: (i) *solver convergence* for a *fixed* truncation, and (ii) *truncation convergence* as the ansatz space is enlarged. Only the first admits a general mathematical proof without problem-specific input; the second is treated here by certification-grade stability diagnostics.

C.1. Newton–Kantorovich Theorem for Fixed Truncations (Proven)

Let $F_N : \mathbb{R}^{n_N} \to \mathbb{R}^{n_N}$ denote the truncated FRG beta-function map (or residual of the fixed-point equation) at truncation order N. A fixed point $g_N^\star$ satisfies $F_N(g_N^\star) = 0$.

Theorem 6 (Newton–Kantorovich (finite-dimensional form))**.** *Let $F : \mathbb{R}^n \to \mathbb{R}^n$ be continuously differentiable on a convex set U. Assume there exists $g_0 \in U$ such that $DF(g_0)$ is invertible and*

$$\beta := \left\| DF(g_0)^{-1} F(g_0) \right\| < \infty, \qquad L := \sup_{g,h\in U} \frac{\|DF(g) - DF(h)\|}{\|g-h\|} < \infty. \tag{C1}$$

If $2\beta L < 1$ and the closed ball $B(g_0, r)$ with $r = \frac{1-\sqrt{1-2\beta L}}{L}$ is contained in U, then Newton iteration $g_{m+1} = g_m - DF(g_m)^{-1}F(g_m)$ is well-defined, converges to a unique root $g^\star \in B(g_0, r)$, and satisfies $\|g_m - g^\star\| \leq 2^{-m} r$.

Proof. This is the standard Newton–Kantorovich theorem; a self-contained proof follows from contraction mapping applied to the Newton map, using the Lipschitz control of DF and invertibility at g_0. $\square$

C.2. Truncation Convergence and κ_{eff} as Certified Interval (Certified-Numerical/External-Datum)

The nontrivial question is whether $g_N^\star$ converges as $N \to \infty$ to an exact FRG fixed point in function space, and whether observables are stable under regulator variation. Absent a functional analytic proof for the full QICT-motivated truncation class, we adopt a conservative certification posture:

 doi:10.20944/preprints202512.2120.v1

- **Proven:** solver convergence and uniqueness for each fixed truncation, whenever the Newton–Kantorovich hypotheses can be verified numerically (condition number and Lipschitz diagnostics).
- **Certified numerical:** stability plateaus under (a) regulator sweeps, (b) truncation-order sweeps, and (c) solver tolerance sweeps, producing an interval estimate for κ_{eff}.
- **External datum (allowed):** if plateau stability fails, κ_{eff} must be treated as an external input with an explicit likelihood model.

In the present bundle, κ_{eff} is propagated as an interval defined in `QICT_Canonical_Constants.json` and audited by the PASS/FAIL contract.

D. Blueprint for a 3D Gauge-Coded Unitary QCA Embedding (Conjecture)

This appendix provides a concrete, locality-preserving circuit architecture that upgrades the 1D Dirac-limit toy model to a 3D lattice gauge dynamics with gauge group $SU(3) \times SU(2) \times U(1)$. It is *not* claimed as a finished derivation of the full Standard Model; rather, it shows that the QICT "microscopic language" (finite-range unitary updates with a Gauss-law code subspace) admits a native 3D non-Abelian generalization.

D.1. Local Hilbert Spaces and Gauss-Law Code Subspace

Let $\Lambda \subset \mathbb{Z}^3$ be a cubic lattice. On each site $x \in \Lambda$, let $\mathcal{H}_x^{\text{mat}}$ carry fermionic matter fields in the desired representations (three generations can be included by tensoring three copies). On each oriented link (x, μ) with $\mu \in \{\hat{x}, \hat{y}, \hat{z}\}$, let $\mathcal{H}_{x,\mu}^G$ carry a finite-dimensional *quantum link* (or other finite-dimensional gauge-field truncation) for each gauge factor $G \in \{SU(3), SU(2), U(1)\}$.

Define local Gauss generators G_x^a (for each Lie algebra component a) acting on $\mathcal{H}_x^{\text{mat}} \otimes_\mu \mathcal{H}_{x,\mu}^G \otimes_\mu \mathcal{H}_{x-\mu,\mu}^G$. The physical code subspace is

$$\mathcal{H}_{\text{phys}} := \{|\psi\rangle : G_x^a|\psi\rangle = 0 \ \forall x, a\}. \tag{D1}$$

D.2. Gauge-Invariant Finite-Depth Update

A single QCA time step is defined as a finite-depth circuit

$$U := U_E \, U_B \, U_F, \tag{D2}$$

where U_E is a product of on-link "electric" rotations, U_B is a product of plaquette "magnetic" rotations, and U_F is a product of gauge-covariant fermion hopping gates. A standard choice (Trotterized lattice gauge dynamics) is:

$$U_E := \prod_{x,\mu} \exp\left(-\mathrm{i}\alpha \, E_{x,\mu}^2\right), \tag{D3}$$

$$U_B := \prod_{\square} \exp\left(-\mathrm{i}\beta \, \mathrm{Re}\,\mathrm{Tr}\, U_\square\right), \tag{D4}$$

$$U_F := \prod_{x,\mu} \exp\left(-\mathrm{i}\gamma \left(\psi_x^\dagger U_{x,\mu} \psi_{x+\mu} + \text{h.c.}\right)\right), \tag{D5}$$

with couplings (α, β, γ) and where $U_\square$ is the ordered product of link operators around the plaquette $\square$. Each layer is manifestly gauge invariant and therefore preserves $\mathcal{H}_{\text{phys}}$:

$$U \, \mathcal{H}_{\text{phys}} = \mathcal{H}_{\text{phys}}. \tag{D6}$$

The continuum limit (and chiral-fermion realization) requires additional structure (e.g. domain-wall or Ginsparg–Wilson-type constructions), but the circuit-level locality and Gauss-law protection are compatible with the QICT axioms.

 doi:10.20944/preprints202512.2120.v1

D.3. Status and What Would "Close" This Block

To promote this blueprint from CONJECTURE to PROVEN/CERTIFIED-NUMERICAL, one would need (i) an explicit finite-dimensional gauge-field truncation with controlled continuum limit, (ii) a demonstrably chiral light sector, and (iii) numerical/analytic control of transport properties (diffusion/Drude suppression) in the protected charge sector. These requirements are *independent* of the micro–macro closure logic in the main text and can be audited modularly.

References

1. J. M. Deutsch, Phys. Rev. A **43**, 2046 (1991).
2. M. Srednicki, Phys. Rev. E **50**, 888 (1994).
3. A. Polkovnikov, K. Sengupta, A. Silva, and M. Vengalattore, Rev. Mod. Phys. **83**, 863 (2011).
4. A. Nahum, S. Vijay, and J. Haah, Phys. Rev. X **8**, 021014 (2018).
5. C. W. von Keyserlingk, T. Rakovszky, F. Pollmann, and S. L. Sondhi, Phys. Rev. X **8**, 021013 (2018).
6. A. Chan, A. De Luca, and J. T. Chalker, Phys. Rev. X **8**, 041019 (2018).
7. F. G. S. L. Brandão, A. W. Harrow, and M. Horodecki, Local random quantum circuits are approximate polynomial-designs, Commun. Math. Phys. **346**, 397 (2016).
8. D. A. Levin, Y. Peres, and E. L. Wilmer, *Markov Chains and Mixing Times* (American Mathematical Society, 2009).
9. G. Vidal, Efficient classical simulation of slightly entangled quantum computations, Phys. Rev. Lett. **91**, 147902 (2003).
10. G. Vidal, Efficient simulation of one-dimensional quantum many-body systems, Phys. Rev. Lett. **93**, 040502 (2004).
11. S. Popescu, A. J. Short, and A. Winter, Entanglement and the foundations of statistical mechanics, Nat. Phys. **2**, 754 (2006).
12. S. Sugiura and A. Shimizu, Thermal pure quantum states at finite temperature, Phys. Rev. Lett. **108**, 240401 (2012).